Single-walled carbon nanotube growth using $[Fe_3(\mu_3\text{-}O)(\mu\text{-}O_2CR)_6(L)_3]^{n+}$ complexes as catalyst precursors†‡

Douglas Ogrin,[a] Ramon Colorado, Jr.,[a] Benji Maruyama,[b] Mark J. Pender,[b] Richard E. Smalley[a,c] and Andrew R. Barron*[a]

Received 13th September 2005, Accepted 25th October 2005
First published as an Advance Article on the web 9th November 2005
DOI: 10.1039/b512885d

We present herein the VLS growth of SWNTs from oxo-hexacarboxylate–triron precursors, $[Fe_3O(O_2CCH_3)_6(EtOH)_3]$ (**1**) and $[Fe_3O(O_2CCH_2OMe)_6(H_2O)_3][FeCl_4]$ (**2**), on spin-on-glass surfaces, using C_2H_4/H_2 (750 °C) and CH_4/H_2 (800 and 900 °C) growth conditions. The SWNTs have been characterized by AFM, SEM and Raman spectroscopy. The characteristics of the SWNTs are found to be independent of the identity of the precursor complex or the solvent from which it is spin-coated. The as grown SWNTs show a low level of side-wall defects and have an average diameter of 1.2–1.4 nm with a narrow distribution of diameters. At 750 and 800 °C the SWNTs are grown with a range of lengths (300 nm–9 μm), but at 900 °C only the longer SWNTs are observed (6–8 μm). The yield of SWNTs per unit area of catalyst nanoparticle decreases with the growth temperature. We have demonstrated that spin coating of molecular precursors allows for the formation of catalyst nanoparticles suitable for growth of SWNTs with a high degree of uniformity in the diameter, without the formation of preformed clusters of a set diameter.

Introduction

The growth of carbon nanotubes from supported catalyst particles occurs by vapor–liquid–solid (VLS) growth,[1] that is believed to occur *via* two mechanistic steps: nucleation and growth.[2,3] Nucleation involves both the formation of a catalyst particle and the initial construction of the carbon framework on which the tube is later grown. At growth temperatures the catalyst metal atoms aggregate to form a liquid metal nanoparticle. For the growth of single walled carbon nanotubes (SWNTs), it is proposed that the nanoparticle needs to consist of *ca.* 50–200 metal atoms (1–100 nm).[4] The size of this particle has been proposed to have an effect on the diameter and type (as defined by the SWNT's *m*,*n* value) of tube produced.[4–6] Although evidence for this postulate is limited, it is an attractive research goal that specific catalysts (or catalyst precursors) can be designed to provide a specific *m*,*n* SWNT or at least a limited range of SWNT types.

A variety of transition-metal catalysts and alloys have been studied. The metals most commonly used for SWNT growth are iron, cobalt, nickel, molybdenum, and various bimetallic alloys of these metals.[7] Irrespective of the metal source, catalysts that enable narrow size and chirality distributions in SWNT production (with a high yield, *i.e.*, SWNT : catalyst ratio) are desired since polydispersed metal nanoparticle catalysts result in SWNTs with a wide size distribution. Several approaches have been made to prepare catalysts with highly controlled size distribution in the hope of synthesizing SWNTs with narrow diameter distributions, including, the use of supports,[8] diblock copolymer micelles,[9] ferritin[5,10] and dendrimers.[11] These supports are usually treated with an iron salt, and then annealed to form Fe_2O_3 nanoparticles. Arrays of posts and strips, patterned into a thermally evaporated iron surface, have also shown success.[12] In a recent publication Liu and co-workers have shown the iron–molybdenum nanocluster $[H_xPMo_{12}O_{40}\subset H_4Mo_{72}Fe_{30}(O_2CMe)_{15}O_{254}(H_2O)_{98}]$ (FeMoC) to be a suitable catalyst precursor for the growth of SWNTs.[13]

We are interested in the application of small molecular precursors for VLS growth of uniform SWNTs, in particular, on surfaces. Our rationalization for the use of the small molecular precursors was based upon two questions. First, if a simple molecular species is used as the catalyst precursor what control over SWNT diameter is possible? It has been postulated that preformed clusters of a set diameter (without aggregation) are required for surface VLS growth of SWNTs with uniform diameters. An individual molecule as a precursor can be assumed to be too small for seeding SWNT growth. Thus, either aggregation of the precursor on the surface or aggregation of the metal atoms after reduction must occur in order to generate a cluster of sufficient size. If aggregation were random, then a wide range of catalyst cluster sizes, and therefore distribution of SWNT diameters would be expected. Second, can the crystal packing/intermolecular forces between different molecular clusters be used as a route to fabrication of catalyst particles with different sizes?

In choosing a suitable class of precursor the following points were considered: high yield synthesis allowing for solubility in a wide range of solvents through different functional groups,

[a]*Department of Chemistry and Center for Nanoscale Science and Technology, Rice University, Houston, Texas, 77005, USA. E-mail: arb@rice.edu*
[b]*Materials and Manufacturing Directorate, Air Force Research Laboratory, Wright Patterson AFB, Ohio, 45433, USA*
[c]*Carbon Nanotechnology Laboratory, Rice University, Houston, Texas, 77005, USA*

† Electronic supplementary information (ESI) available: Fig. S1: TGA plot for **2**. Fig. S2: A SEM micrograph of SWNTs grown on SOG substrate from **1** using CH_4/H_2 (1 : 1) at 800 °C. Fig. S3: Plot of percentage of active catalysts as a function of growth temperature. See DOI: 10.1039/b512885d

‡ Dedicated to the memory of our recently departed colleague, Richard E. Smalley. He will be sorely missed.

and multiple metal atoms without being of sufficient size to form a nanocluster on their own. The oxo-hexacarboxylate–triron compounds, $[Fe_3(\mu_3\text{-}O)(\mu\text{-}O_2CR)_6(L)_3]^{n\pm}$, fulfill these needs. These compounds contain either $[Fe(III)_3]$, $[Fe(III)_2Fe(II)]$, or $[Fe(III)Fe(II)_2]$ cores depending on whether the complex is cationic, neutral, or anionic, respectively.[14] Derivatives may be prepared with a range of both carboxylate substituents and neutral donor ligands, and many of the examples have been crystallographically characterized. The oxo-hexacarboxylate–triron compounds are too small to act as catalyst precursors and therefore the formation of a catalyst particle will require aggregation. The desire to produce an EtOH or H_2O soluble derivative for attachment to a functionalized SWNT prompted the synthesis of $[Fe_3O(O_2CMe)_6(EtOH)_3]$ (**1**) and $[Fe_3O(O_2CCH_2OMe)_6(H_2O)_3][FeCl_4]$ (**2**). We have previously shown that methoxyacetic acid derived nanoparticles show good solubility in water and alcohols.[15]

We present herein the VLS growth of SWNTs from $[Fe_3(\mu_3\text{-}O)(\mu\text{-}O_2CR)_6(L)_3]^{n+}$ precursors on spin-on-glass surfaces. The effects of precursor identity ($n = 0$, 1), carbon source (CH_4 *vs.* C_2H_4), and growth temperature (750–900 °C), on the uniformity and yield of SWNTs are discussed.

Results and discussion

The EtOH soluble acetate derivative, $[Fe_3O(O_2CMe)_6(EtOH)_3]$ (**1**) was prepared by solvent exchange from the aquo-complex, $[Fe_3O(O_2CMe)_6(H_2O)_3]$.[16] Reaction of $FeCl_3$ with methoxyacetic acid/$NaHCO_3$ in water allowed for the isolation of dark red crystals of $[Fe_3O(O_2CCH_2OMe)_6(H_2O)_3][FeCl_4]$ (**2**). The structure of **2** has been confirmed by X-ray crystallography.[17] The choice of both neutral and ionic complexes was aimed at determining the effects of solvent (and therefore evaporation rates) during spin coating of the catalyst precursor. In addition, the crystal structure of compound **2** exhibits an extended structure in which the clusters are linked by intra-trimer hydrogen bonding to form a zigzag motif that form sheets *via* hydrogen bonding involving disordered waters of hydration. The $[FeCl_4]^-$ anion is intercalated between the hydrogen-bonded sheets.[17] The aggregation of compound **2** should be dominated by hydrogen bonding and ion interactions, while that of compound **1** is only reliant on van der Waals interactions. Thus, the aggregation of compound **2** should be favored over the aggregation of compound **1**. Finally, the presence of chlorine in a catalyst precursor has been thought to be detrimental to SWNT growth unless prior thermolysis to Fe_2O_3 is accomplished.

Dilute solutions (0.1 mM) of compounds **1** and **2** were prepared in EtOH and H_2O, respectively, and spin-coated onto silicon wafer substrates coated with a spin-on-glass (SOG) layer (see Experimental section). The SOG is used to provide a smooth, uniform surface. The choice of 0.1 mM solutions was to allow for sufficient precursor to be deposited without formation of micron sized crystals or precursor that result in the formation of multi wall carbon nanotubes (MWNTs). The samples were placed in the hot zone of Mullite tube mounted in an electric tube furnace, and subjected to a three-step growth process: thermolysis, reduction and growth.

Decomposition of the precursors was accomplished by heating to the desired growth temperature under argon. The thermogravimetric analysis (TGA) of compounds **1** and **2** under argon show thermolysis *via* loss of coordinated solvent ligands followed by decomposition up to 300 °C. Compound **2** loses one equivalent of Fe per formula (presumably as chloride) between 750 and 950 °C. Thus, nanoparticles prepared from compound **2** when heated to 750 °C will contain chlorine which will allow for a comparison of the possible effects of chlorine in the precursor.

Reduction of the iron oxide features at under a hydrogen atmosphere (see below) was followed by the introduction of the growth gas and cessation of the argon flow. Three growth gas/temperature conditions were explored. Ethylene has been found to be a feedstock for growth at lower temperatures, while methane generally provides cleaner growth, *i.e.*, in the absence of amorphous carbon. Although prior experiments with molecular precursors and CH_4 have generally been run at 900 °C we chose to also study lower temperature growth. This was for two reasons. First, this temperature is the upper limit for the growth chamber for *in-situ* Raman monitoring, and second, it allows for a comparison with the C_2H_4 growth. A summary of growth conditions is given in Table 1.

The growth of SWNTs is confirmed by AFM measurements of the diameters of the SWNTs (Table 1) and more importantly by *in-situ* Raman spectroscopy within a growth chamber for samples grown from compound **1** in CH_4/H_2 at 800 °C (see Experimental section). As may be seen from Fig. 1, the spectra of the surface before and after a growth run indicate the appearance of the tangential band (G-band) at 1590 cm^{-1} that is characteristic of a SWNT. The lack of a disorder band (D) band) at *ca.* 1350 cm^{-1} which indicates sp^3 hybdrization on the sidewalls, is evidence that the SWNTs grown have very few defects and low sidewall functionalization.[18]

Scanning electron microscopy (SEM) of the surface after growth for samples grown at 750 and 800 °C clearly show the presence of features consistent with SWNT growth (*e.g.*, Fig. 2). Samples grown from CH_4/H_2 at 900 °C show only sparse coverage. AFM allows for more detailed analysis of the samples.

Table 1 Summary of SWNT growth experiments

Precursor/solvent[a]	Growth gas	T^d/°C	Average SWNT diameter[e]/nm	SWNT length range[e]/μm	Yield (%)[f]
1/EtOH	C_2H_4/H_2[b]	750	1.2 ± 0.2	0.3–7	30–50
1/EtOH	CH_4/H_2[c]	800	1.3 ± 0.2	0.3–6	15–25
1/EtOH	CH_4/H_2[c]	900	1.4 ± 0.3	6–8	1–2
2/H_2O	C_2H_4/H_2[b]	750	1.3 ± 0.2	0.5–9	30–50
2/H_2O	CH_4/H_2[c]	800	1.3 ± 0.2	0.3–6	15–25
2/H_2O	CH_4/H_2[c]	900	1.4 ± 0.3	6–8	1–2

[a] 10^{-4} M. [b] Gas ratio of 1 : 4. [c] Gas ratio of 1 : 1. [d] All samples heated to growth temperature under Ar. All growth runs of 15 min. [e] Measured by AFM. [f] Number of SWNTs grown per catalyst feature in a 1 μm × 1 μm square.

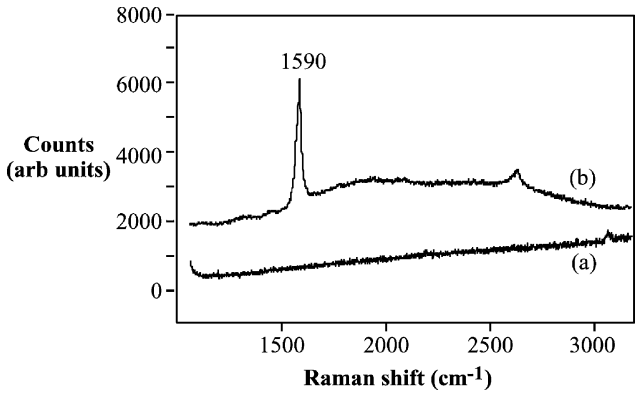

Fig. 1 Raman spectra of sample (a) before and (b) after growth run with $[Fe_3O(O_2CCH_3)_6(EtOH)_3]$ (**1**) using CH_4/H_2 (1 : 1) at 800 °C.

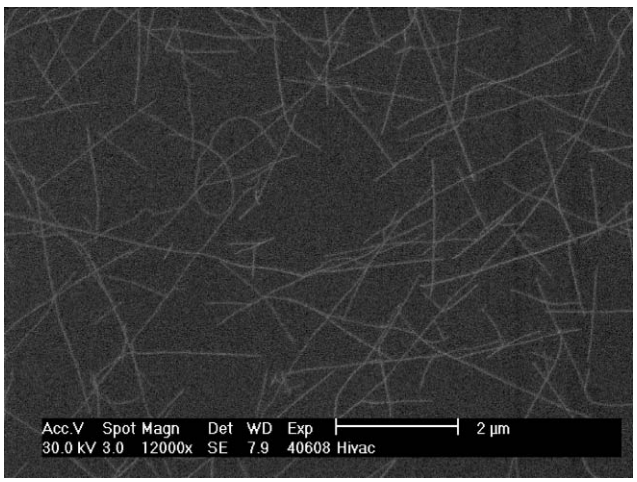

Fig. 2 A representative SEM micrograph of SWNTs grown on SOG substrate from $[Fe_3O(O_2CCH_2OMe)_6(H_2O)_3][FeCl_4]$ (**2**) using CH_4/H_2 (1 : 1) at 800 °C.

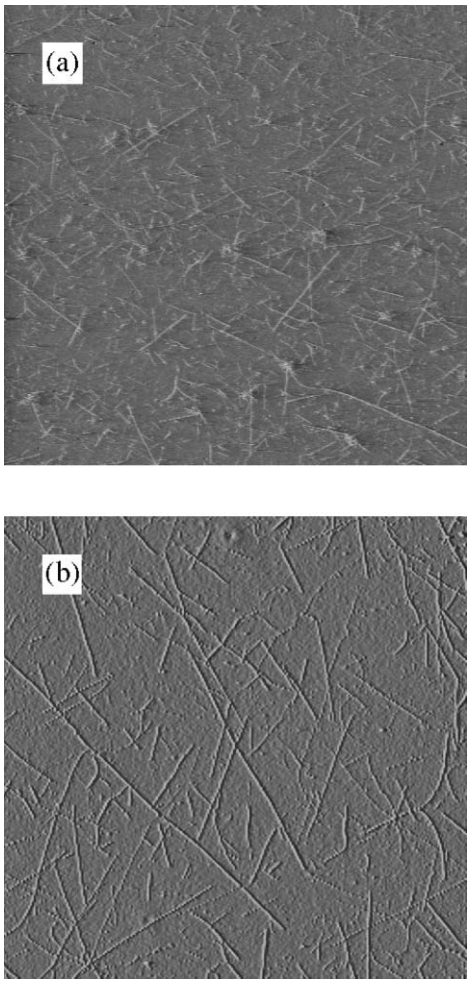

Fig. 3 Representative AFM image of SWNTs grown from (a) $[Fe_3O(O_2CCH_3)_6(EtOH)_3]$ (**1**) and (b) $[Fe_3O(O_2CCH_2OMe)_6(H_2O)_3][FeCl_4]$ (**2**) using C_2H_4/H_2 (1 : 4) at 750 °C. Images are 10 × 10 µm.

Fig. 3 shows representative AFM images of SWNTs grown from compounds **1** and **2** using C_2H_4/H_2 growth conditions. It may be clearly seen that there is a high proportion of SWNTs per catalyst feature suggesting that the majority of catalyst particles formed from the catalyst precursor are active for SWNT growth. The similarity of results for compounds **1** and **2** suggest that the presence of chloride ligands in the precursor is not a detriment to SWNT growth. Based upon the analysis of catalyst particles *vs*. SWNTs grown over a series of 1 × 1 µm squares analyzed by AFM, there is no difference in activity between the catalysts formed from $[Fe_3O(O_2CMe)_6(EtOH)_3]$ in EtOH and $[Fe_3O(O_2CCH_2OMe)_6(H_2O)_3][FeCl_4]$ in H_2O (Table 1). Samples grown using CH_4/H_2 at 800 °C show a slightly lower coverage (Fig. 4) to that observed with C_2H_4/H_2 (Fig. 3). However, it is worth noting that the range of length of the grown SWNT remains essentially constant (Table 1). This would suggest that despite the higher temperatures and different growth gases the growth rates are unchanged but the fraction of active catalysts decreases (to 15–25% @ 800 °C). The fraction of active catalysts decreases significantly for the CH_4/H_2 growth at 900 °C (see Table 1). The number of active catalysts decreases exponentially with increased temperature. Samples grown at 900 °C using CH_4/H_2 show very few SWNTs per unit area compared to the number of catalyst particles (Fig. 5). Although the average lengths of the SWNTs grown at 900 °C are much longer (6–8 µm) than those grown at lower temperatures (300 nm, ~9 µm), the SWNTs grown at 900 °C appear to be identical to the longest grown at lower temperatures, *i.e.*, the maximum growth rates are unchanged with temperature. We propose that increasing the growth temperature does not significantly alter the growth rate due to the feedstock-limited conditions (*i.e.*, the relative concentrations of CH_4 or C_2H_4 and H_2) under which these experiments were conducted. Nevertheless, increasing the temperature does deactivate a significant fraction of the catalyst particles.

The above results demonstrate that in this system the growth of SWNTs is independent of the identity of the catalyst precursor and the solvent it is spin-coated from. An explanation of this observation is obtained by a consideration of the size of the catalyst particles formed upon the thermolysis and reduction of the catalyst precursor molecules. Fig. 6 shows AFM images of samples of **1** and **2** spin-coated onto SOG substrates after reduction with H_2 at 900 °C. The catalyst nanoparticles formed from the reductive decomposition of compounds **1** and **2** on SOG are 8.0 ± 1.0 nm and 9.0 ± 0.3 nm, respectively. Despite the differences

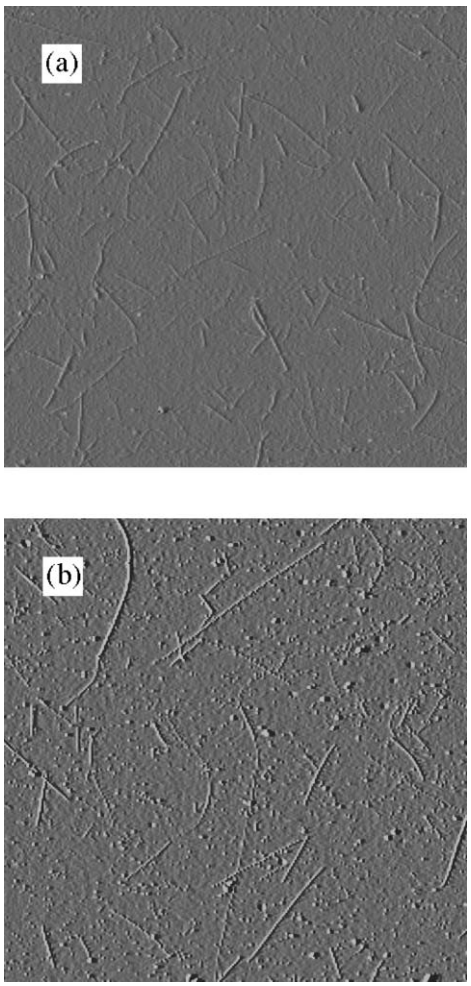

Fig. 4 Representative AFM image of SWNTs grown from (a) $[Fe_3O(O_2CCH_3)_6(EtOH)_3]$ (**1**) and (b) $[Fe_3O(O_2CCH_2OMe)_6(H_2O)_3][FeCl_4]$ (**2**) using CH_4/H_2 (1 : 1) at 800 °C. Images are 5 × 5 μm.

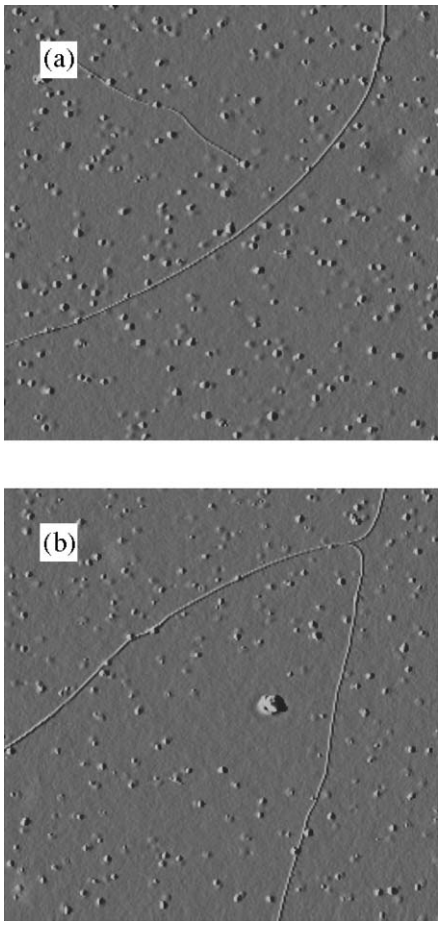

Fig. 5 Representative AFM image of long SWNT grown from (a) $[Fe_3O(O_2CCH_3)_6(EtOH)_3]$ (**1**) and (b) $[Fe_3O(O_2CCH_2OMe)_6(H_2O)_3][FeCl_4]$ (**2**) using CH_4/H_2 (1 : 1) at 900 °C. Images are 2 × 2 μm.

in the catalyst precursor compound solubilities and solid-state aggregation (van der Waals interactions *vs*. hydrogen bonding), upon reduction with H_2 at 900 °C the resulting Fe catalyst particles are remarkably similar. We note that these particles are significantly larger than observed for previous constrained precursors. Thus, irrespective of the identity of the precursor complex or the solvent the resulting catalyst particles are of comparable size. This suggests that for the SOG surfaces, diffusion and surface tension effects control the catalyst size.

As noted in the Introduction the size of the catalyst particle has been proposed to have an effect on the diameter and type (as defined by the SWNT's *m*,*n* value) of tube produced.[4–6] In this regard, previous researchers have postulated that in order for SWNTs to be grown with narrow distribution of diameters constrained sized catalysts or single molecular catalysts must be employed. In the present work, we have shown that irrespective of the identity of the precursor or its solid-state structure,[17] or the solvent from which it is deposited, similar and uniformly sized catalyst particles are obtained. Furthermore, as may be seen from Table 1 the diameter of the resulting SWNTs are within a narrow range. It should be noted that the percentage standard deviation (15–21%) is significantly lower than observed for SWNTs grown from the 2 nm diameter molecular nanocluster $[H_xPMo_{12}O_{40} \subset H_4Mo_{72}Fe_{30}(O_2CMe)_{15}O_{254}(H_2O)_{98}]$ (38%).[13]

The size distributions for SWNTs grown from $[Fe_3O(O_2CMe)_6(EtOH)_3]$ and $[Fe_3O(O_2CCH_2OMe)_6(H_2O)_3][FeCl_4]$ using C_2H_4/H_2 at 750 °C and CH_4/H_2 at 800 °C are shown in Fig. 7. A consideration of the average SWNT diameter (Table 1) as a function of precursor and/or growth conditions suggests that there is some effect of these parameters the size distribution plots. However, from Fig. 7 there is a slight shift towards larger diameter for the higher temperature runs, but the statistical significance of this is questionable. We propose that the size distribution of the SWNTs is essentially independent of the growth temperature/gas and the precursor. It should be noted that given the paucity of SWNTs on each wafer for the CH_4/H_2 @ 900 °C growth runs the sample size is insufficient to allow good statistics.

As noted in the Introduction, it has been proposed that the diameters of SWNTs are proportionally related to the sizes of the catalytic nanoparticles used in the surface VLS growth process.[4–6] It should be noted that some of the evidence for this proposal is based upon results with MWNTs.[6] A consequence of this proposal has been the search for precursor particles constrained to a small size and narrow size distribution.[11,13,19–21] Our present results using molecular complexes that are themselves too small to grow SWNTs without aggregation, show that large catalyst

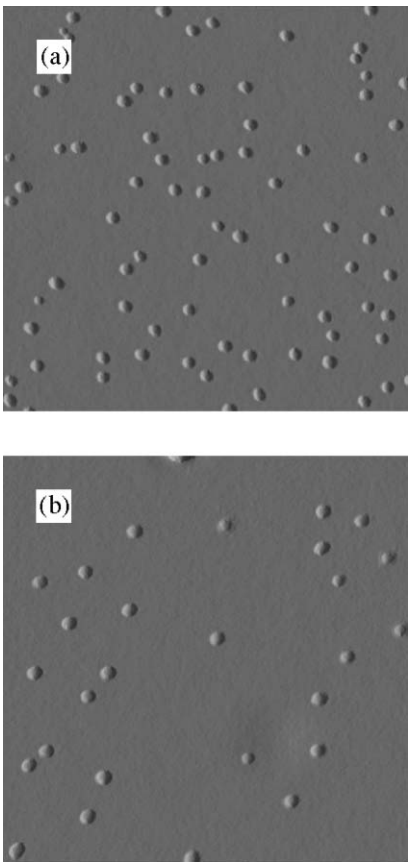

Fig. 6 Representative AFM image of Fe nanoparticle catalysts formed from the reductive decomposition of spin-coated (a) $[Fe_3O(O_2CCH_3)_6(EtOH)_3]$ (**1**) and (b) $[Fe_3O(O_2CCH_2OMe)_6(H_2O)_3][FeCl_4]$ (**2**). Images are 1×1 μm.

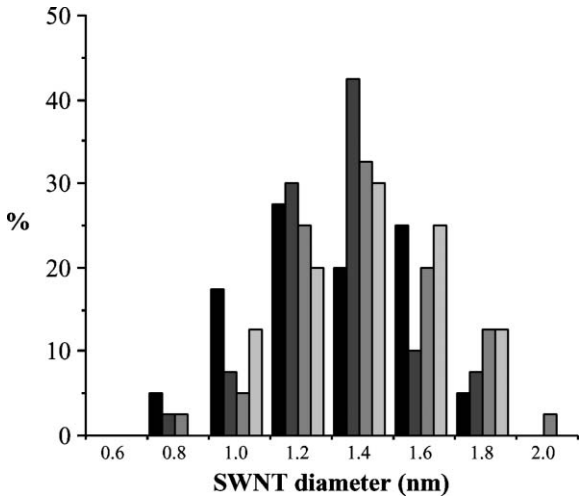

Fig. 7 Diameter distribution of the SWNTs grown from $[Fe_3O(O_2CCH_3)_6(EtOH)_3]$ (**1**) using C_2H_4/H_2 (1:4) at 750 °C (black) or CH_4/H_2 (1 : 1) at 800 °C (dark grey) and $[Fe_3O(O_2CCH_2OMe)_6(H_2O)_3][FeCl_4]$ (**2**) using C_2H_4/H_2 (1 : 4) at 750 °C (grey) or CH_4/H_2 (1 : 1) at 800 °C (light grey).

nanoparticles (8–9 nm) allow for the growth of SWNTs with diameters comparable to prior results with smaller nanoparticles. Fig. 8 shows a plot of SWNT diameter as a function of catalyst nanoparticle size for VLS growth from iron catalysts. All values were obtained using AFM measurements. It can be seen that (with the exception of precursors forming bundles or MWT, see below) catalyst precursors between 1 and 9 nm result in a moderate range of SWNT diameters (0.8–1.5 nm). Our results suggest that controlling the size of the catalyst nanoparticle is not necessary for the growth of SWNTs with a small diameter and a narrow distribution and that simple unconstrained molecular precursor offer as much control over the SWNT growth than constrained precursors. We note that the published AFM data for the two values in Fig. 8 that appear to show increased SWNT diameter with increased catalyst size (formed using $FeCl_3$/poly(2-vinylpyridine)[21] and Fe-doped apoferritin[19]) show evidence for the formation of bundles or ropes. It is not clear that this effect or the formation of MWNTs is responsible for the apparent large diameter range. In this regard, we note that if during spin coating of compounds **1** or **2** large micron sized crystals are formed then MWNT are formed in place of SWNTs (Fig. 9).

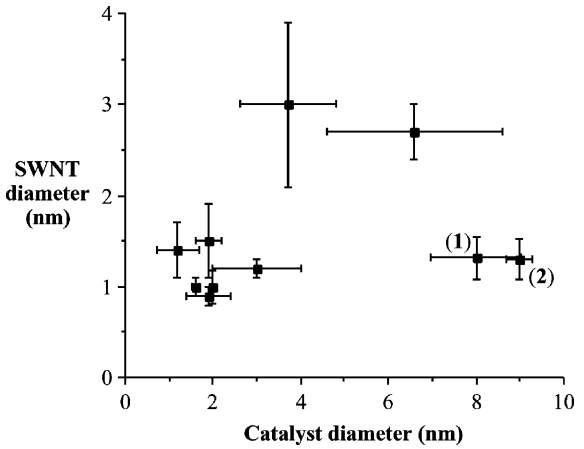

Fig. 8 Plot of catalyst diameter with deviation *vs.* the diameter of the SWNTs grown on a surface by VLS from the Fe-containing catalyst using CH_4/H_2 growth gas. Based upon known diameters for SWNTs it is expected that bundles (ropes) would have a diameter >2 nm. Values for SWNTs grown from compounds **1** and **2** indicated.

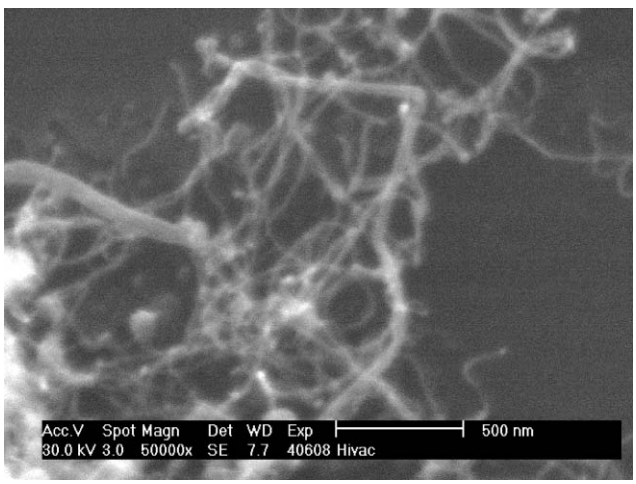

Fig. 9 A representative SEM micrograph of MWNTs grown from $[Fe_3O(O_2CCH_3)_6(EtOH)_3]$ (**1**) using C_2H_4/H_2 (1 : 4) at 750 °C.

Given that the rate of precursor decomposition (for a given precursor, *i.e.*, CH_4 *vs*. C_2H_4) and C–C bond formation should be constant for a given catalyst (Fe) the rate of SWNT growth should be constant between individual SWNTs if initiation events occur simultaneously. An interesting observation of a unique feature gives insight to the "catalyst nucleation" and "growth" steps in growth. Fig. 10 shows an AFM image of two SWNTs that have grown from two catalyst particles (labeled) and have bisected at the same point in space. The SWNTs are similar in diameter and the initial catalyst particle may be seen from their relative height to be positioned at the open ends of the "V". The intersection of the two SWNTs does not show any catalyst, precluding the possibility that two SWNTs grew from a single catalyst particle. The similarity in lengths suggest that in order for mutual termination to occur at the same point on the surface, the nucleation and growth of the SWNT must have occurred at the same time and rate. This would suggest that any catalyst particle that is going to be active is activated at the initial stages of the growth reaction. If it does not initiate growth it will not do so at a later time. It also suggests that given similar surface interactions (roughness, obstacles, *etc.*) the SWNTs will grow at the same rate.

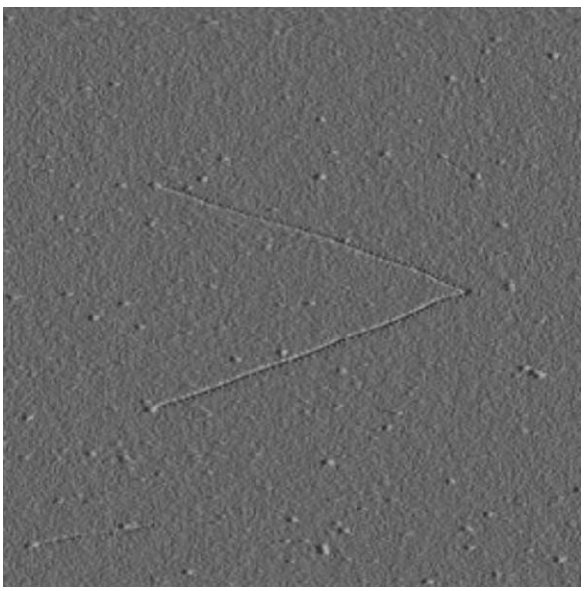

Fig. 10 AFM image of two SWNTs mutually terminated during the growth from $[Fe_3O(O_2CCH_2OMe)_6(H_2O)_3][FeCl_4]$ (**2**) using CH_4/H_2 (1 : 1) at 800 °C. Image is 3 × 3 μm.

Finally, observation of Figs. 3–5 shows that the shorter SWNTs (<1 μm) are straight, while the longest SWNTs (6–8 μm) gently curve. We propose the straight SWNTs are a result of growth along the surface (Fig. 11(a)) while the longer SWNTs are formed by growth out of the plane of the surface (Fig. 11(b)). The growth rate of the former will be limited due to SWNT $\cdots$ SiO_2 surface interactions, while the latter will have unrestricted growth away from the surface. Once the reaction run is complete (and the gas flow is removed) the SWNTs grown out of the surface will fall over, resulting in the images shown in Figs. 3–5. We propose that, in the absence of additional factors, the rate of SWNT growth is reduced by a factor of *ca.* 8 due to the interaction with the surface. This proposal suggests a further question. Why are the catalysts that result in surface parallel growth (Fig. 11(a)) the ones deactivated with increased temperatures while those resulting in surface-free growth (Fig. 11(b)) appear to be stable to higher temperatures? Furthermore, why are a significant fraction of catalysts inactive even at relatively low growth temperatures? In order to investigate these questions we are continuing our studies in the area of surface catalyst interactions.

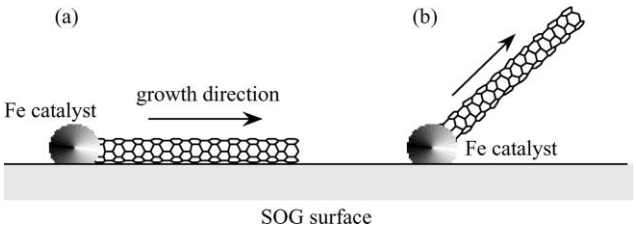

Fig. 11 Schematic representation of supported catalyst SWNTs growth in which the SWNT grows parallel to the surface (a) or out from the surface (b).

Conclusions

We have demonstrated that SWNTs can been grown using simple molecular iron precursors, $[Fe_3O(O_2CMe)_6(EtOH)_3]$ and $[Fe_3O(O_2CCH_2OMe)_6(H_2O)_3][FeCl_4]$ spin-coated onto a SOG substrate. The advantages of this class of precursor is the ease of synthesis of various substituents allowing for control over solubility, that in-turn allows for spin coating onto substrates from a wide range of solvents.

While the relative activity of SWNT growth appears to be independent of the precursor and possibly the growth gas, there is clearly a dependence on the growth temperature. At 900 °C there is a marked deactivation of the catalysts since inactive catalyst particles are still seen on the surface along with the grown SWNTs. Interestingly, the catalysts that remain active are those that grow the longest SWNTs. It has been proposed that the formation of an amorphous carbon coating is the likely cause of this inactivation of the catalyst particles at high temperature.[19] However, given the complex interplay of catalyst activation, nucleation, growth, and termination the reasons why the 'most active' catalysts remain active at higher temperatures, but the catalysts with apparently lower activity cease under the same condition are unclear. We propose that a future goal of surface VLS growth of SWNTs is an understanding of the apparent low overall activity of catalyst particles.

We have demonstrated that spin coating of molecular precursors allows for the formation of catalyst nanoparticles suitable for growth of SWNTs with a high degree of uniformity in the diameter, without the formation of preformed clusters of a set diameter. Unfortunately, the crystal packing/intermolecular forces between different molecular clusters do not appear to provide a route to controlling the SWNT diameter. The result of this present work questions the ability of particular sized precursor particles to determine the diameter of the SWNTs grown from those particles. While this does not offer hope for designed catalysts for SWNT growth, it does suggest that a single catalyst precursor may be used in the amplification of preformed SWNTs irrespective of their *m*,*n* values. Our research in this area is continuing.

Experimental

$Fe_3O(O_2CCH_3)_6(H_2O)_3$ was prepared according to a previously reported method.[16] Methoxyacetic acid (Aldrich), acetic acid (Fisher), sodium bicarbonate (Fisher), 200 proof EtOH (Pharmco), and $FeCl_3{\cdot}6H_2O$ (Alfa Aesar) were ACS reagent grade or better and used as received. Spin-on-glass was purchased from Honeywell and used as received. Thermal gravimetric analysis was carried out on a Seiko TG/DTA 200. Atomic force microscopy measurements were obtained using a Digital Instruments NanoScope IIIa scanning probe microscope in tapping mode. A RTESP type Nanoprobe™ SPM Tip with a drive frequency of 300 kHZ was used. Tips were replaced frequently to ensure the accuracy of the images and limit tip artifacts. Images were taken at a scan frequency of 1–2 Hz and 256–512 samples line^{-1}. Scanning electron micrographs were obtained on a FEI XL30 without a conductive coating.

$[Fe_3O(O_2CMe)_6(EtOH)_3]$ (1)

$[Fe_3O(O_2CMe)_6(H_2O)_3]$ (500 mg, 0.845 mmol) was suspended in EtOH (100 mL). The solution was heated to reflux for 2 h, at which time the solution became a deep red, and all solids dissolved. The solution was cooled to room temperature and the volatiles were removed *in vacuo* to give a brick red solid. Yield: 475 mg, 95%. UV-vis: 203 nm and 310 nm. IR (cm^{-1}): 3379 (m, OH), 2966 (m), 1594 [m, $\nu_{as}(COO^-)$], 1410 [s, CO_2], 1345 (w), 1260 (m), 1092 (m), 1026 (m), 800 (w) and 657 (Fe_3O).

$[Fe_3O(O_2CCH_2OMe)_6(H_2O)_3][FeCl_4]$ (2)

Methoxyacetic acid (5.87 g, 65.2 mmol) was slowly added to an aqueous solution of sodium bicarbonate (5.46 g, 65.2 mmol). The solution was gently heated until the effervescence (CO_2) ceased. The solution was added dropwise to an aqueous solution of $FeCl_3{\cdot}6H_2O$ (8.81 g, 32.6 mmol). The reaction was stirred for 4 h at room temperature. The solvent was removed *in vacuo* to give a dark red powder. Yield: 80%, 8.40 g. UV-vis (H_2O): $\lambda = 204$ ($\varepsilon =$ 21157 L mol^{-1} cm^{-1}) and 282 ($\varepsilon = 5979$ L mol^{-1} cm^{-1}) nm. IR: 3338 (m, OH), 2931 (m), 2831 (m), 1596 (s, CO_2), 1440 (s, CO_2), 1409 (s), 1198 (s, asym. OCH_3), 1116 (s, sym. OCH_3), 941 (m), 919 (m), 708 (m, Fe_3O) cm^{-1}.

VLS Growth from $[Fe_3O(O_2CR)_6(L)_3]^{n\pm}$

A Thermolyne 211000 tube furnace with a mullite tube and plumbed with purified gases was used for the growth runs. Flow rates were 150 sccm for Ar and 225 sccm for both CH_4 and H_2. An n-type 100 silicon wafer was coated with a 100 nm layer of spin-on-glass (Accuglass® T111) and was cured at in air 700 °C for 1 h, and then cut into 1 cm^2 pieces. By varying spin speed, it is possible to obtain thickness from 86–360 nm. A 150 nm thick layer was used for our catalyst samples by spinning at 2000 rpm for 30 s. A solution (0.1 mM) of the appropriate precursor was prepared. A drop of the solution was spin coated onto the wafer at 3,000 rpm for 40 s. The silicon wafer with catalyst was placed in a quartz boat and positioned within the hot zone of the tube furnace. Ar gas (150–1000 sccm) was flowed over the sample as it was heated to the growth temperature (Table 1) at a rate of 10–30 °C min^{-1}. The growth run began when the Ar was replaced with CH_4 (225 sccm, 99.9%) and H_2 (225 sccm) for 15 min. The system was then cooled to room temperature under Ar. With these flow rates; the formation of amorphous carbon was not a problem. Flow rates for runs using C_2H_4 and H_2 were 100 sccm and 400 sccm, respectively.

In-situ Raman growth was performed on a TS1500 Hotstage from Linkam Scientific Instruments Ltd. fitted to a Renishaw InVia(tm) Raman microscope, and plumbed with UHP gases was used for the growth runs at atmospheric pressure. Flow rates were 15 sccm for argon and 100 sccm for both methane and hydrogen. A drop of solution of $[Fe_3O(O_2CMe)_6(EtOH)_3]$ was spin coated onto the wafer at 3000 rpm for 40 s. The silicon wafer with catalyst was placed in the well of the stage's ceramic heating element. The stage was flushed with argon as the temperature was raised to 800 °C at 10 °C.min^{-1}. Once at temperature, the hydrogen and methane were turned on, followed by the argon being turned off. The growth run lasted for 15 min, after which the argon was turned back on, and the hydrogen and methane turned off. The stage was allowed to cool to room temperature. With these flow rates; the formation of amorphous carbon was not observed by visual observation of the heating element, or from significant Raman D peak intensity. Before, during and after growth, Raman spectra were acquired using a 514 nm Ar Ion laser with a rated power of 150 mW. The laser power delivered to the sample is normally 4.8 mW, however this was somewhat reduced due to transmission losses through the sapphire window of the hotstage. Spectra taken at the growth temperature were not useful due to excessive thermal background.

Acknowledgements

Financial support for this work is provided by the Robert A. Welch Foundation and the Defense Advanced Research Projects Agency (DARPA).

References

1 E. F. Kukovitsky, S. G. L'vov and N. A. Sainov, *Chem. Phys. Lett.*, 2000, **317**, 65.
2 J. Gavillet, A. Loiseau, F. Ducastelle, S. Thair, P. Bernier, O. Stéphan, J. Thibault and J.-C. Charlier, *Carbon*, 2002, **40**, 1649.
3 A. Gorbunov, O. Jost, W. Pompe and A. Graff, *Carbon*, 2002, **40**, 113.
4 F. Ding, A. Rosén and K. Bolton, *J. Chem. Phys.*, 2004, **121**, 2775.
5 Y. Li, W. Kim, Y. Zhang, M. Rolandi, D. Wang and H. Dai, *J. Phys. Chem. B*, 2001, **105**, 11424.
6 C. L. Cheung, A. Kurtz, H. Park and C. M. Leiber, *J. Phys. Chem. B*, 2002, **106**, 2429.
7 F. Banhart, N. Grobert, M. Terrones, J.-C. Charlier and P. M. Ajayan, *Int. J. Mod. Phys. B*, 2001, **15**, 4037.
8 M. Su, B. Zheng and J. Liu, *Chem. Phys. Lett.*, 2000, **322**, 321.
9 Q. Fu, S. Huang and J. Liu, *J. Phys. Chem. B*, 2004, **108**, 6124.
10 Y. Zhang, Y. Li, W. Kim, D. Wang and H. Dai, *Appl. Phys. A*, 2002, **74**, 325.
11 H. C. Choi, W. Kim, D. Wang and H. Dai, *J. Phys. Chem. B*, 2002, **106**, 12361.
12 H. B. Peng, T. G. Ristroph, G. M. Schurmann, G. M. King, J. Yoon, V. Narayanamurti and J. A. Golovchenko, *Appl. Phys. Lett.*, 2003, **83**, 4238.
13 L. An, J. M. Owens, L. E. McNeil and J. Liu, *J. Am. Chem. Soc.*, 2002, **124**, 13688.
14 S. G. Shova, I. G. Cadelnic, M. Gdaniec, Y. A. Simonov, T. C. Jovmir, V. M. Meriacre, G. Filoti and C. I. Turta, *J. Struct. Chem.*, 1998, **39**, 747; R. A. Reynolds, III, W. R. Dunham and D. Coucouvanis, *Inorg. Chem.*, 1998, **37**, 1232.

15 R. L. Callender, C. J. Harlan, N. M. Shapiro, C. D. Jones, D. L. Callahan, M. R. Wiesner, R. Cook and A. R. Barron, *Chem. Mater.*, 1997, **9**, 2418; C. T. Vogelson and A. R. Barron, *J. Non-Cryst. Solids*, 2001, **290**, 216.
16 M. K. Johnson, R. D. Cannon and D. B. Powell, *Spectrochim. Acta, Part A*, 1982, **38**, 307.
17 D. Ogrin, S. G. Bott and A. R. Barron, *J. Chem. Crystallogr.*, 2006, in press.
18 M. S. Dresselhaus, M. A. Pimenta, P. C. Ecklund and G. Dresselhaus, *Raman Scattering in Materials Science*, ed. W. H. Webber and R. Merlin, Springer-Verlag, Berlin, 2000.
19 Y. Li, W. Dim, Y. Zhang, M. Rolandi, D. Wang and H. Dai, *J. Phys. Chem. B*, 2001, **105**, 11424.
20 R. M. Kramer, L. A. Sowards, M. J. Pender, M. O. Stone and R. R. Naik, *Langmuir*, 2005, **21**, 8466.
21 Q. Fu, S. Huang and J. Liu, *J. Phys. Chem. B*, 2004, **108**, 6124.

